Optimisation of pH of cadmium chloride post-growth-treatment in processing CDS/CDTE based thin film solar cells

OJO, A. A. and DHARMADASA, I <http://orcid.org/0000-0001-7988-669X>

Published version

OJO, A. A. and DHARMADASA, I (2017). Optimisation of pH of cadmium chloride post-growth-treatment in processing CDS/CDTE based thin film solar cells. Journal of Materials Science: Materials in Electronics, 28 (10), 7231-7242.

OPTIMISATION OF pH OF CADMIUM CHLORIDE POST-GROWTH-TREATMENT IN PROCESSING CdS/CdTe BASED THIN FILM SOLAR CELLS

A.A. Ojo* and I.M. Dharmadasa

Electronic Materials and Sensors Group, Materials and Engineering Research Institute (MERI), Sheffield Hallam University, Sheffield S1 1WB, UK.

*Email: chartell2006@yahoo.com; Tel: +44 114 225 6910 Fax: +44 114 225 6930

ABSTRACT

The role of Chlorine-based activation in the production of high quality CdS/CdTe photovoltaic have been well discussed and explored with an overlook of the effect of Cadmium chloride ($CdCl_2$) post-growth treatment acidity on the property of the fabricated devices. This work focuses on the optimisation of $CdCl_2$ post-growth treatment pH as it affects both the material and fabricated device properties of all-electrodeposited multilayer glass/FTO/*n*-CdS/*n*-CdTe/p-CdTe configuration. $CdCl_2$ treatments with acidity ranging from pH1 to pH4 were explored. The properties of the ensued CdTe layer were explored using optical, morphological, compositional structural and electrical property analysis, while, the effect on fabricated multilayer glass/FTO/*n*-CdS/*n*-CdTe/p-CdTe configuration were also explored using both I-V and C-V measurements. Highest improvements in the optical, morphological, compositional and structural were observed at pH2 $CdCl_2$ post-growth treatment with an improvement in absorption edge, grain size, crystallinity and crystallite size. Conductivity type conversions from n-CdTe to p-CdTe, increase in pin-hole density and collapse of the absorption edge were observed after pH1 $CdCl_2$ treatment. The highest fabricated solar cell efficiency of 13% was achieved using pH2 $CdCl_2$ treatment as compared to other pH values explored.

Keywords: CdS/CdTe; pH; post-growth-treatment; cadmium chloride treatment

1 INTRODUCTION

Although efficiency stagnation in the cadmium sulphide/cadmium telluride (CdS/CdTe) based solar cell has been reported in the literature for the past twenty years prior to the recent improvement in both material and processing issues, post-growth treatment (PGT) has been documented as one of the most important processing step towards enhancing solar to electrical energy conversion efficiency. With properties such as grain growth, recystallisation, improved stoichiometry, grain boundary passivation, optimisation of doping concentration [1] among other advantages attributed to the PGT of CdS/CdTe, PGT has been the focus of many researchers. Although research focus has been turned towards identifying the best chlorine-based gas or salt solution either in aqueous or methanol in which the highest efficiency can be achieved [2]–[6], the best application method [7] and also the optimisation of both annealing temperature and time [8]. So far, the effects of the pH values of the chlorine salt solution have been often overlooked. With emphasis on cadmium chloride ($CdCl_2$) PGT, this paper focuses on the effect of PGT solution treatment pH on both the material and device properties of CdS/CdTe based solar cell. Both the CdS and the CdTe layers were grown using two-electrode electrodeposition configuration due to its simplicity.

2 EXPERIMENTAL DETAILS

2.1 SAMPLE PREPARATION

All the conducting substrates and chemicals used in this set of experiments were procured from Sigma-Aldrich, United Kingdom. As it is a requirement for electrodeposition to utilise a conducting substrate, the TEC7 glass/fluorine-doped tin oxide (glass/FTO) substrate utilised are strips of 5×4 cm^2 area with a sheet resistance 7 Ω/□. The strips of glass/FTO were washed in an ultrasonic bath containing soap solution for 15 minutes. The substrates were rinsed thoroughly in deionised (DI) water and degreased using hydrocarbons such as methanol and acetone. The substrates were rinsed afterwards in running DI water and directly transferred into the cadmium sulphide electrolytic bath.

2.1.1 CdS BATH PREPARATION AND GROWTH

The cadmium sulphide electrolytic bath contains 0.12 M cadmium chloride hydrate ($CdCl_2 \cdot xH_2O$) with a purity of 99.995% and 0.18 M ammonium thiosulphate ($(NH_4)_2S_2O_3$) with a purity of 99% in 400 ml of DI water. The aqueous electrolytic solution was contained in a 500 ml polypropylene beaker placed inside an 800 ml glass beaker. A small quantity of DI water is contained in the outer glass beaker for uniform heating of the electrolytic

bath contained within the glass beaker. Prior to deposition, the pH of the electrolytic bath was adjusted to 2.50± 0.02 using dilute ammonium hydroxide (NH_4OH) and dilute hydrochloric (HCl) acid to increase or reduce the pH value of the bath respectively. The deposition temperature and stirring rate were adjusted to 85°C and ~300 rpm respectively. It should be taken into consideration that intrinsically, CdS is always *n*-type due to defects such as Cd interstitials and S vacancies within the lattice. CdS was deposited at a pre-optimised cathodic voltage of 1200 mV based on structural, optical, morphological, compositional and electrical property evaluation of CdS as documented in the literature [9]. 120 nm thick CdS layer was grown on the glass/FTO strip. The glass/FTO/*n*-CdS layer was heat treated at 400°C for 20 minutes. The absence of $CdCl_2$ from the treatment at this stage was to isolate the effect of post-growth-treatment pH and the inclusion of $CdCl_2$ on the characteristic properties of the CdS/CdTe-based solar cell, as it is well known that CdS properties improve after the inclusion of $CdCl_2$ in PGT. After heat treatment, the glass/FTO/*n*-CdS layer was rinsed in running DI water to wash off loose Cd, S and CdS which has been reported in the literature as detrimental to fabricated solar devices [10]. The glass/FTO/*n*-CdS layers were transferred into the cadmium telluride (CdTe) bath immediately afterwards.

2.1.2 CdTe BATH PREPARATION AND GROWTH

The cadmium telluride electrolytic bath contains 1.5 M cadmium nitrate tetrahydrate $Cd(NO_3)_2{\cdot}4H_2O$ with a purity of 99.995%, 0.03 M of tellurium oxide (TeO_2) with a purity of 99.995% and 800 ml DI water bath. The electrolytic aqueous solution was contained in a 1000 ml polypropylene beaker and housed in an external 1800 ml glass beaker similar to the CdS bath configuration. Before the growth of CdTe, the pH, growth temperature and stirring rate were set to 2.00±0.02, 85°C and ~300 rpm respectively. It should be noted that CdTe can intrinsically be *n*-, *i*- or *p*- conduction type based on the atomic concentration of Cd and Te. With a higher atomic concentration of Te to Cd, a *p*-CdTe layer is grown while *n*-CdTe can be grown with a higher concentration of Cd to Te [11]. Based on the pre-optimisation CdTe using structural, optical, morphological, compositional and electrical evaluation as described by Salim et al., 2015 [12]. Within the experimental constrain of this work, stoichiometric CdTe was observed at 1370 mV while both the *n*-CdTe and *p*-CdTe for these set of experiments were grown at 1375 mV and 1365 mV respectively. Utilising a continuous deposition process, 1200 nm thick *n*-CdTe followed by a 30 nm thick *p*-CdTe were grown to achieve glass/FTO/*n*-CdS/*n*-CdTe/*p*-CdTe configuration. The incorporation of the comparatively thin *p*-CdTe layer was necessitated to pin the Fermi level close to the valence band and also to reduce the contact resistance at the metal-semiconductor

interface [13]. However, an increase in the *p*-CdTe thickness in this configuration causes a detrimental effect on the device parameters due to deep junction formation [6].

2.1.3 POST-GROWTH-TREATMENT PREPARATION AND APPLICATION

Post-growth-treatment commences immediately after the growth of CdTe resulting into glass/FTO/*n*-CdS/*n*-CdTe/*p*-CdTe configuration. The glass/FTO/*n*-CdS/*n*-CdTe/*p*-CdTe layer is rinsed in DI water to remove loose Cd, Te or CdTe and later dried in a stream of nitrogen gas. The 5×4 cm^2 glass/FTO/*n*-CdS/*n*-CdTe/*p*-CdTe was cut into 5 strips (of 1×4 cm^2 area) from the glass-side, rinsed thoroughly in running DI water to wash off glass shrapnel and dried in a stream of nitrogen gas.

Prior to the application of $CdCl_2$ treatment, 0.1 M $CdCl_2$ was dissolved in 80 ml of DI water in a 100 ml glass beaker at room temperature. To achieve homogeneity, the solution was stirred for 60 minutes and 20 ml of the solution was poured into 4 different 25 ml glass beaker. The beakers were labelled A to D with the solution contained in beaker A being the most acidic with a pH of 1±0.02, beaker B with pH 2±0.02, beaker C with pH 3±0.02 and beaker D was left as-prepared with pH of ~4.02±0.02. It should be noted that the acidity level of the $CdCl_2$ solution contained in the 25 ml beaker were adjusted using dilute HCl.

$CdCl_2$ solution with different pH treatment were applied by adding few droplets on each strip labelled A to D at this point based on the pH of the solution in which they were treated while the fifth strip E was left as-deposited. Each strip was allowed to air dry before heat treating at 420°C for 20 minutes in air except the as-deposited strip E. Afterwards, each strip of glass/FTO/*n*-CdS/*n*-CdTe/*p*-CdTe layers was rinsed in running DI water, dried in stream of nitrogen gas and etched using solution containing potassium dichromate ($K_2Cr_2O_7$) and concentrated sulphuric acid (H_2SO_4) for acid etching and a solution containing sodium hydroxide (NaOH) and sodium thiosulfate ($Na_2S_2O_3$) for basic etching for the duration of 5 seconds and 2 minutes respectively to improve the metal/semiconductor contact [14], [15]. 100 nm thick gold (Au) contacts were evaporated on the glass/FTO/*n*-CdS/*n*-CdTe/*p*-CdTe using a 3 mm diameter mask. The fabricated devices were analysed using both current-voltage and capacitance-voltage characteristic measurements to determine their device parameters. (It should be noted that the $CdCl_2$ post-growth-treatment referred to in this paper denotes $CdCl_2$ treatment and heat treatment at 420°C for 20 minutes in air.)

2.2 EXPERIMENTAL TECHNIQUE

To ascertain the effect of $CdCl_2$ treatment pH on the all-electroplated glass/FTO/*n*-CdS/*n*-CdTe/*p*-CdTe layers, the optical, morphological, compositional structural and electrical properties were analysed. The optical properties were analysed using Cary 50 Scan Ultraviolet-Visible (UV-Vis) spectrophotometer at room temperature within the wavelength range of 400 nm to 1000 nm. Prior to measurements, the baseline was set using a blank TEC7 glass/FTO to eliminate its effect on the obtained result. Both the scanning electron microscopy (SEM) for morphological analysis and the energy-dispersive X-ray spectroscopy (EDX) for compositional analysis of the layers were carried out using FEI Nova 200 NanoSEM equipment at a magnification of ×60,000. The structural analysis in which information such as crystallite size and phase identification were obtained using Philips PW 3,710 X'pert diffractometer with Cu-Kα monochromator of wavelength λ=1.54 Å. For this set of experiments, both the generator tension and current were adjusted to 40 kV and 40 mA respectively. The conductivity types of the grown layers after post-growth-treatment were determined using photoelectrochemical (PEC) cell measurement. Robust technique such as Hall effect measurement was not possible due to the embedded transparent conducting substrate (fluorine doped tin oxide) on which the semiconductor layers were grown.

After metallisation with Au contacts, the electrical properties of the fully fabricated glass/FTO/*n*-CdS/*n*-CdTe/*p*-CdTe/Au cells were measured using automated Rera Solution PV simulation system. Prior to measurements using the solar simulating system, the system was calibrated using standard RR267MON Si-based solar cell at room temperature.

3 RESULTS AND DISCUSSION

3.1 OPTICAL PROPERTY ANALYSIS

Further to the experimental details as discussed in Section 2.2, Figure 1 (a) shows the Tauc's plot [16] of $\left(\alpha hc/\lambda\right)^2$ against photon energy $\left(hc/\lambda\right)$, where α is absorption coefficient h is the plank's constant, c is the speed of light and λ is the wavelength. Figure 1 (b) shows the graph of absorption edge slope against the $CdCl_2$ post-growth-treatment pH. The optical energy bandgap of the as-deposited and the $CdCl_2$ treated CdTe layers were obtained by extrapolating the linear portion of the curve to $\left(\alpha hc/\lambda\right)^2$ =0. From observation, it could be said that the optical bandgap lies within the 1.45±0.01 eV for the as-deposited and all the $CdCl_2$ treated CdTe layers. This observed bandgap shows comparability with the standard bulk CdTe bandgap of 1.45 eV. More

importantly, the absorption edge slope as shown in Figure 1 (b) can be related to semiconductor layer quality as discussed in the literature [5], [17]. As expected, an improvement in the absorption edge of the as-deposited glass/FTO/*n*-CdS/*n*-CdTe was observed after $CdCl_2$ treatment at different pH. This improvement in attributes have been well documented in the literature [1], [2], [7]. The steepest absorption edge slope was observed at pH2 while the lowest absorption edge slope was observed at pH1. This reduction in the absorption edge slope might be due to the reduction in the quality of the glass/FTO/*n*-CdS/*n*-CdTe layer as a result of the harshness of the acidic $CdCl_2$ treatment by possible dissolution of Cd from CdTe at high acidity. It should be noted that only the bandgap of CdTe was observable rather than that of the incorporated *n*-CdS layer nor the bowing CdS/CdTe effect [18] due to the thickness of the CdTe layer.

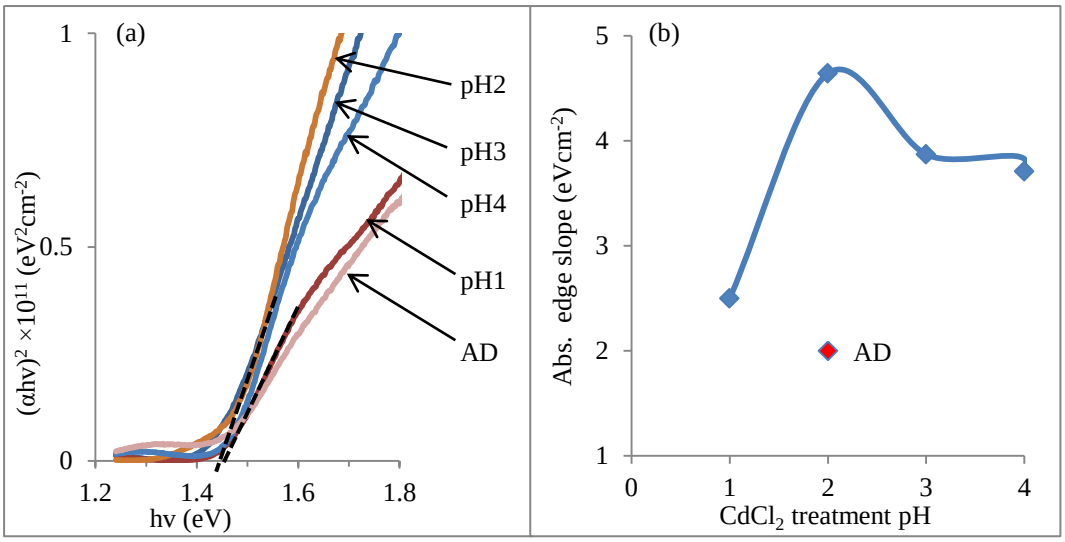

Figure 1: (a) Optical absorption spectra for electrodeposited glass/FTO/n-Cds/n-CdTe thin-films treated with different $CdCl_2$ at different pH values (b) absorption edge slope against PGT $CdCl_2$ pH CdTe thin films

3.2 MORPHOLOGICAL AND COMPOSITIONAL ANALYSIS

Figure 2 (a–d) show the scanning electron microscope (SEM) micrographs of glass/FTO/n-CdS/n-CdTe in the as-deposited, $CdCl_2$ treated at pH1, pH2 and pH4 respectively, while, Figure 2 (e–f) show the energy-dispersive X-ray (EDX) spectra of point identification on the glass/FTO/*n*-CdS/*n*-CdTe treated with pH1 $CdCl_2$ solution. The layer treated with pH3 $CdCl_2$ was excluded due to its high comparability of morphological properties with pH4. The as-deposited glass/FTO/*n*-CdS/*n*-CdTe layer as depicted in Figure 2 (a) shows cauliflower-type morphology which is formed by the agglomerations of small grains. Most importantly, full coverage of the underlying glass/FTO/*n*-CdS layers was observed.

After CdTe treatment at all the explored pH in this work, an increase in grain growth was observed, which is in accord with the literature. The layers treated with pH2 $CdCl_2$ showing a slightly bigger grain size as compared to the layers treated with pH4 $CdCl_2$ as shown in Figure 2. The glass/FTO/*n*-CdS/*n*-CdTe layers treated with pH1 $CdCl_2$ as illustrated in Figure 2 (b) shows deterioration of the glass/FTO/*n*-CdS/*n*-CdTe layer with the presence of pinholes and the accumulation of non-uniform strands on the grains.

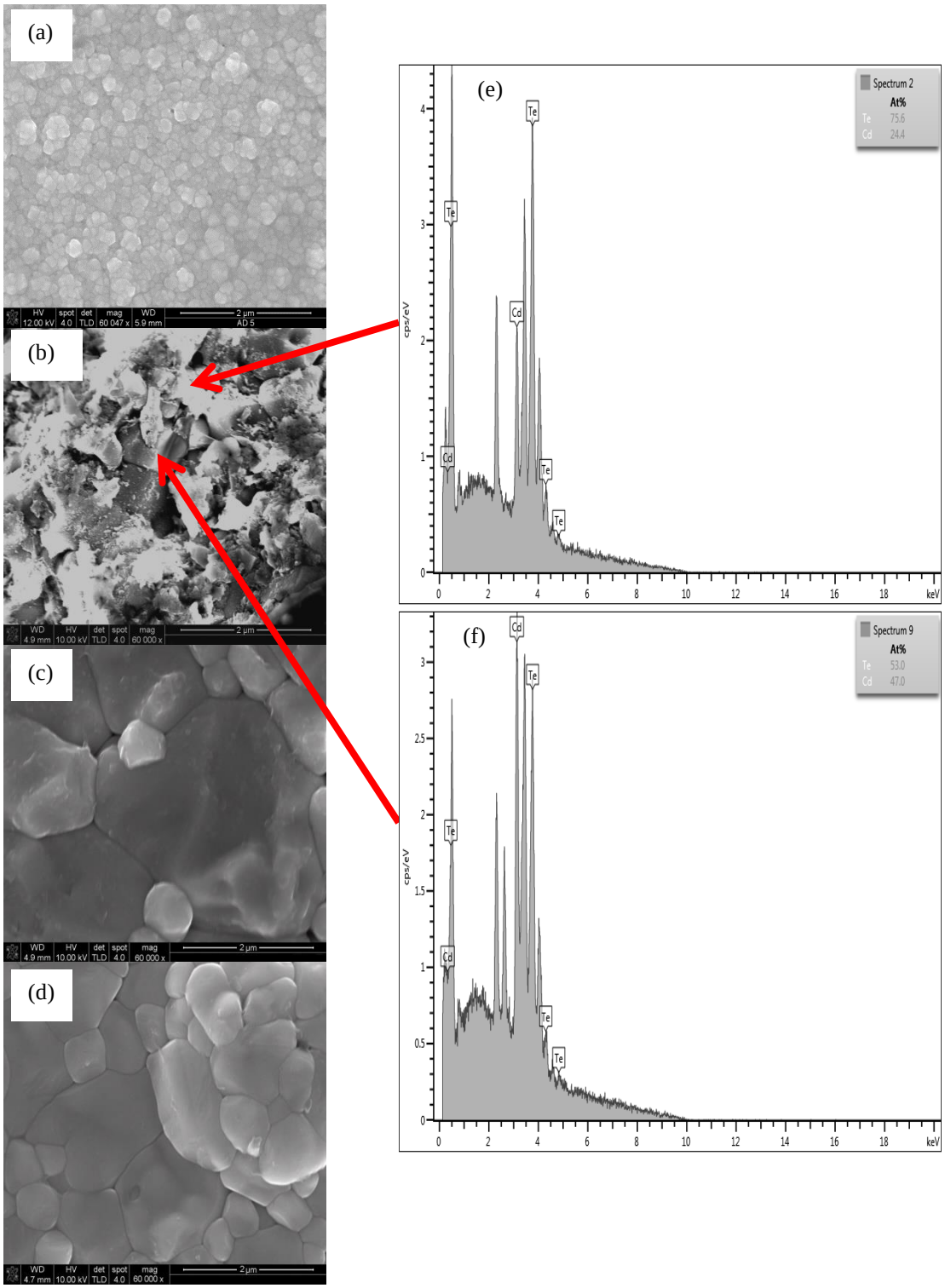

Figure 2: (a) SEM micrograph of as-deposited n-CdTe grown on glass/FTO/n-CdS, (b-d) SEM micrographs for glass/FTO/n-CdS/n-CdTe layers treated with PGT treated with $CdCl_2$ at pH1, pH2 and pH4 respectively, while (e-f) are the EDX point micrograph on layers treated at pH1.

With further investigation on the composition of the strands using EDX as shown in Figure 2 (e-f), it was observed that the strands show an atomic composition of 75.6% for Te and 24.4% for Cd. The presence of the Te-rich strands has also been documented in the literature [19], [20] and as it is well known that an introduction of an acidic media to CdTe attacks Cd leaving rich Te surface [15], [21]. This observation signifies the detrimental effect of pH1 $CdCl_2$ for post-growth-treatment on the material quality of the glass/FTO/*n*-CdS/*n*-CdTe all-electrodeposited layers and may result in the reduction in the device quality.

Figure 3 shows the graph of Cd/Te atomic composition against the acidity of the $CdCl_2$ PGT of glass/FTO/*n*-CdS/*n*-CdTe on a 6×6 μm^2 area obtained using EDX. As shown in Figure 3, reduction in the atomic concentration of Cd was observed after $CdCl_2$ treatment at all the pH explored including for pH1. The reduction in the Cd atomic concentration and shift towards 1:1 ratio of Cd to Te can be attributed to $CdCl_2$ treatment at favourable pH [1]. At pH1, an increase in the Te atomic concentration was observed due to harsh effect of highly acidic $CdCl_2$ on elemental Cd. This observation can be related to the Te-richness obtained after wet acid etching of CdTe layer as reported in the literature [15]

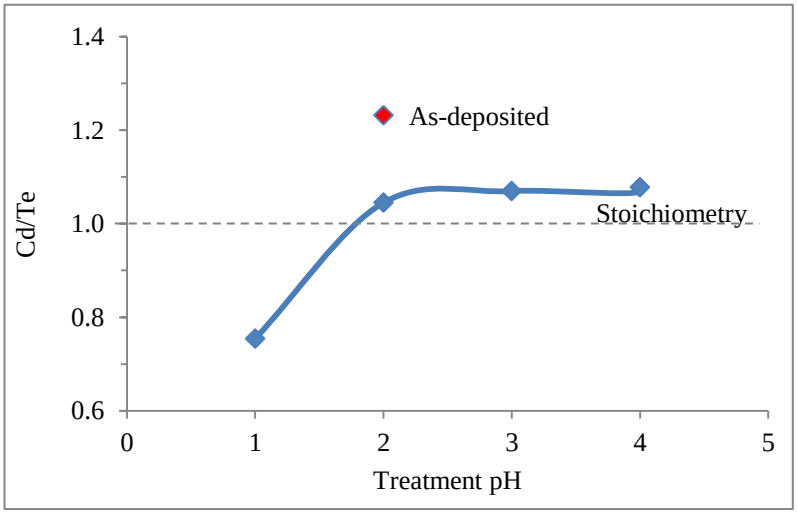

Figure 3: Graphical representation of percentage atomic composition ratio of Cd to Te atoms for $CdCl_2$ treated CdTe layer after different PGT pH as obtained from EDX micrographs.

3.3 STRUCTURAL ANALYSIS

The analysis was aimed at identifying the effect of $CdCl_2$ post-growth-treatment pH on XRD peak intensity, crystallinity, crystallite size, preferred phase and orientation of the glass/FTO/*n*-CdS/*n*-CdTe layers. Figure 4 (a) shows the graph of XRD diffraction intensity of the glass/FTO/*n*-CdS/*n*-CdTe layers treated at different $CdCl_2$ pH against 2θ angle. While Figure 4 (b) shows the graph of XRD peak intensity and crystallite size against $CdCl_2$ post-growth-treatment pH. It should be noted that the stacked XRD micrographs as presented in Figure 4 (a) is to aid the comparability of the peak intensity. From observation, XRD peaks associated with CdTe (111), (220) and (311) in their cubic phase ((111)C, (220)C, (311)C) were observed at angle 2θ≈23.8, 2θ≈38.6° and 2θ≈45.8° respectively asides the FTO peaks at 2θ=25.42, 2θ=33.11, 2θ=36.57, 2θ=55.06, 2θ=61.12 and 2θ=65.06 at all the $CdCl_2$ pH treatment explored. As shown in Figure 4 (a), it is clear that the preferred orientation of CdTe at all the pH explored is along the cubic (111) plane based on the intensity of its diffraction. Furthermore, an increase in diffraction intensity of the (111)C peak was observed with increasing $CdCl_2$ post-growth-treatment acidity. The highest diffraction intensity observed at pH2 and the lowest intensity observed at pH1 as shown in Figure 4 (b).

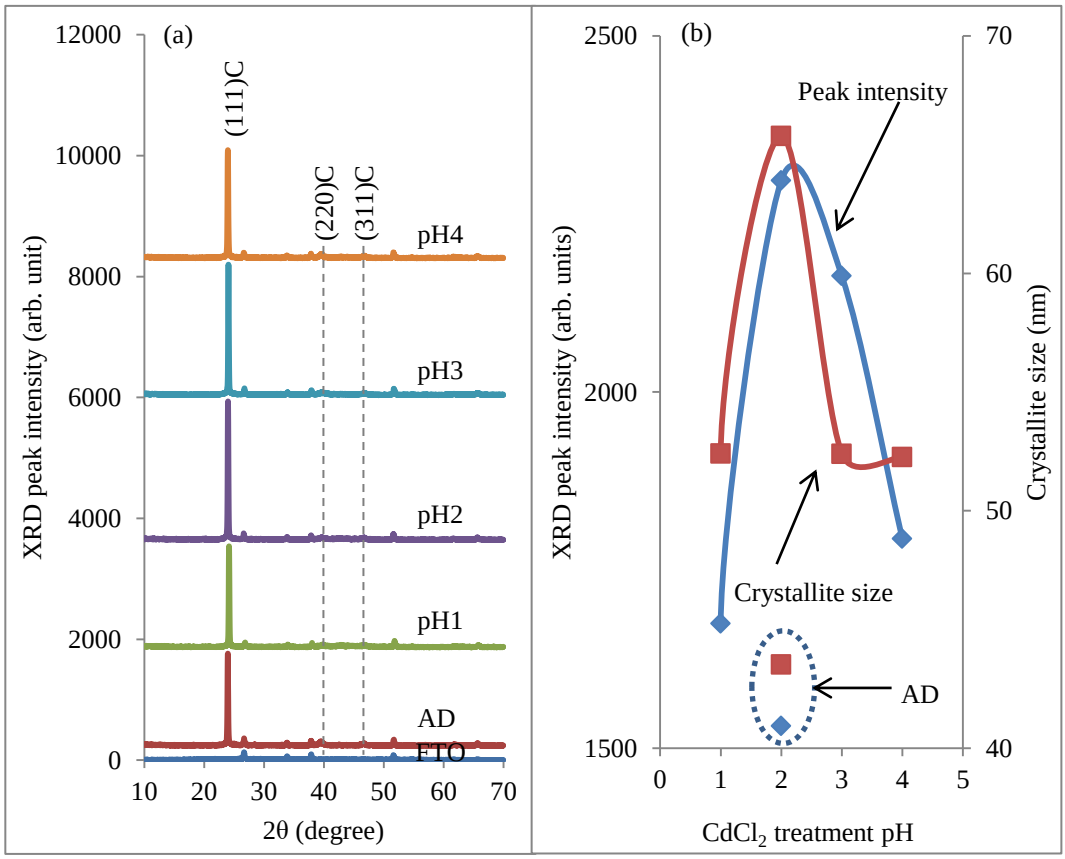

Figure 4: (a) Typical XRD patterns of glass/FTO/n-CdS/n-CdTe layers treated at different $CdCl_2$ pH value (b) typical plot of CdTe (111) cubic peak intensity and crystallite size against $CdCl_2$ post -growth treatment pH value.

This observation can be related to the improvement in the crystallinity of the CdTe layer treated with $CdCl_2$ at pH4, pH3 and pH2 while, the detrimental effects on the CdTe layer crystallinity was observed with increased $CdCl_2$ post-growth-treatment acidity to pH1. This detrimental effect can be further related to harsh etching and sublimation of the CdTe surface, the formation of pinholes, voids, and the formation of CdTe layer rich in Cd or Te with competing phases with CdTe. From observation, no elemental Cd and/or Te peaks were observable in Figure Figure **4** (a) which might be due to possible overlap with FTO peaks, although the formation of elemental Te is most likely as suggested by the compositional analysis in Section 3.2. Based on the preferred cubic (111) CdTe peaks, the crystallite peak was calculated using Scherrer equation as illustrated in Eq (1) , where D is the crystallite size, β is the full width at half maximum (FWHM) of the diffraction peak in radian, θ is the Bragg angle and λ is the wavelength of the X-rays used (1.54 Å).

$$D = \frac{0.94\lambda}{\beta \cos\theta} \tag{1}$$

Table 1 shows the calculated crystallite size and other related properties as obtained from XRD diffraction system. As observed in *Table 1*, the minimum value of the FWHM and the maximum crystallite sizes were attained at pH2. Away from this pH value, a gradually increases in the FWHM and decrease in the crystallite size was observed. This shows further superior quality of $CdCl_2$ post-growth-treatment at pH2 as compared to the other pH explored. It should be noted that the extracted XRD data from these CdTe work matches the International Centre for Diffraction Data (JCPDS) reference file No. 01-775-2086.

Table 1: The XRD analysis of glass/FTO/n-CdS/n-CdTe layers treated with $CdCl_2$ at different pH values

Sample	2θ (degrees)	Lattice Spacing (Å)	FWHM (Degrees)	XRD Peak intensity	Crystallite Size D (nm)	Assignments
AD	23.95	3.7162	0.195	1531	43.52	Cubic
pH1	24.15	3.6812	0.162	1675	52.41	Cubic
pH2	23.99	3.7074	0.129	2297	65.79	Cubic
pH3	24.05	3.6965	0.162	2163	52.40	Cubic
pH4	23.95	3.71485	0.162	1794	52.26	Cubic

3.4 PHOTOELECTROCHEMICAL (PEC) CELL STUDY

The PEC cell measurements were performed by the formation of a solid/liquid junction between the electrodeposited semiconductor and a suitable electrolyte. For this experiment, the electrolyte utilised was a 0.1 M sodium thiosulphate ($Na_2S_2O_3$) dissolved in 20 ml of DI water. Both the semiconductor attached to a high purity graphite rod and the (high purity graphite rod) counter electrodes introduced into the electrolyte were connected to a voltmeter. Due to band bending at the solid/liquid interface as a result of the equalisation of the Fermi level, a Schottky type potential barrier is formed.

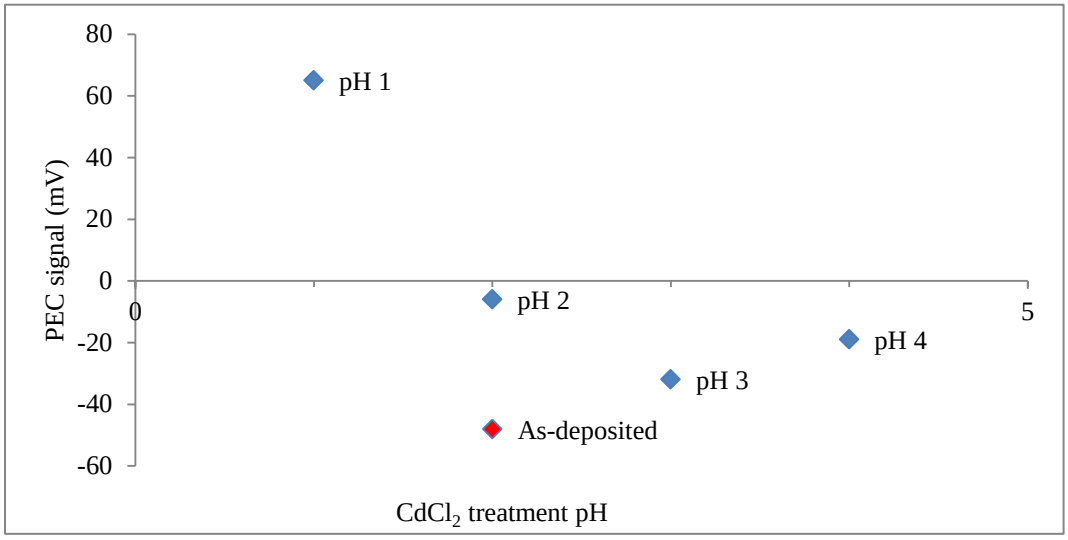

Figure 5: PEC signals for glass/FTO/n-CdTe layers treated with $CdCl_2$ at different pH values.

The direction of flow of the electron is determined by the conductivity type of the semiconductor. The voltage difference (V_L-V_D) between the measured voltage under illuminated condition (V_L) and the measured voltage under dark condition (V_D) determines the conductivity type [22]. The PEC signal sign indicates the conductivity type of the semiconductor layer. A positive voltage difference value is *p*-type, while a negative voltage difference value is an *n*-type semiconductor. Furthermore, PEC signal may give a zero value due to wide bandgap range insulators, overlapping bandgap in conductors (metal) or the mid-gap positioning of the Fermi level in an intrinsic semiconductor.

For this experiment, 1200 nm thick *n*-CdTe was grown at 1375 mV on 4×5 cm^2 glass/FTO. This experiment was performed to ascertain the effect of $CdCl_2$ post-growth-treatment at different pH on the conductivity type of the *n*-CdTe layer utilised in this work. After growth, the glass/FTO/*n*-CdTe layer was cut into five 1×5 cm^2 and treated with $CdCl_2$ at different pH prior to heat treatment at 420°C for 20 minutes as described in Section 2.1.3. Figure 5 shows the graph of PEC signal against as-deposited and post-growth-treated *n*-CdTe at different pH values. As observed from Figure 5, the conductivity type of the as-deposited *n*-CdTe was retained after $CdCl_2$ treatment at pH2, pH3 and pH4 explored in this work with a slight shift towards the opposing conductivity type

except for the layers treated with $CdCl_2$ at pH1. The glass/FTO/*n*-CdTe layer treated with pH1 shows a conductivity type transition into *p*-type. It should be noted that conductivity type conversion after $CdCl_2$ treatment may be due to doping effect caused by heat treatment temperature, duration of treatment, initial atomic composition of Cd and Te, the concentration of $CdCl_2$ utilised in treatment, defect structure present in the starting CdTe layer and the material's initial conductivity type as documented in the literature [1], [6], [12], [23]. Based on these observations coupled with the analysis on composition as discussed in Section 3.2, it could be said that the compositional alteration of the initial *n*-CdTe after pH1 $CdCl_2$ treatment might be one of the determining factors in the conductivity type conversion of the CdTe layers explored in this work. This observation is in accord with the compositional analysis as discussed in Section 3.2.

3.5 DC CONDUCTIVITY STUDY

For this experiment, 1200 nm thick n-CdTe layer was grown on glass/FTO, treated with $CdCl_2$ at different pH after growth and heat treated at 420°C for 20 minutes. On the basis of conductivity type as discussed in Section 3.4, gold (Au) contact was evaporated on the glass/FTO/*p*-CdTe layers, while indium (In) was evaporated on the glass/FTO/*n*-CdTe to form Ohmic contacts prior to the I-V characterisation of the fabricated cells. From the I-V curve generated using Rera Solution PV simulation system, the resistance was calculated as the inverse of the I-V slope and resistivity was calculated as shown in Eq (2) where the calculated resistance R, known contact area A and film thickness L. While the conductivity σ was calculated as an inverse of ρ.

$$\rho = \frac{RA}{L} \tag{2}$$

Table 2 shows the tabulation of properties of the CdTe layers grown on glass/FTO layers and Figure 6 is an illustration of conductivity and resistance against $CdCl_2$ treatment pH. It was observed that an increase in the acidity of the $CdCl_2$ post-growth-treatment solution increases the conductivity of the CdTe layer with saturation observed at ~pH2. Increase in the acidity above pH2 shows a reduction in the conductivity which might be due to the *p*-type conductivity as observed after pH1 $CdCl_2$ treatment as compared to the *n*-type conductivity as observed after pH2, pH3 and pH4 treatment (Section 3.4). It is well known that the conductivity and mobility of an *n*-type semiconductor material are higher than its *p*-type counterpart [24]. Furthermore, increase in the resistivity of the CdTe layer might also be due to CdTe layer deterioration as discussed in Section 3.2.

Table 2: Summary of electrical properties of glass/FTO /n-CdTe layers after $CdCl_2$ treatment at different pH values.

pH	Resistance R (Ω)	Resistivity ρ $\times 10^4$ ($\Omega \cdot$cm)	Conductivity σ $\times 10^{-5}$ ($\Omega \cdot$cm)$^{-1}$
1	42.6	1.12	8.97
2	9.4	0.25	40.63
3	11.3	0.30	33.80
4	15.7	0.41	24.33

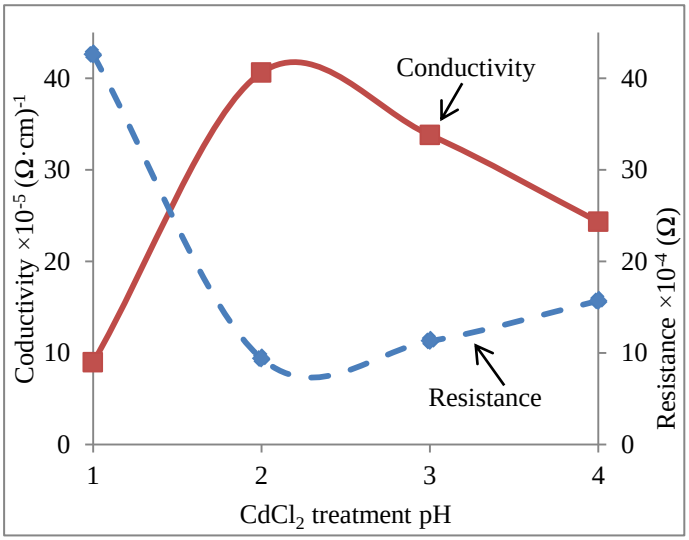

Figure 6: Typical graphs of electrical conductivity and resistance against PGT CdCl2 pH value.

3.6 SOLAR CELL DEVICE CHARACTERISATION

After the optical, morphological, structural and photoelectrochemical properties of the CdTe layers has been analysed, glass/FTO/*n*-CdS/*n*-CdTe/*p*-CdTe/Au devices were fabricated as discussed in Section 2.12.1.3.

3.6.1 CURRENT - VOLTAGE CHARACTERISTICS WITH RECTIFYING CONTACTS

The I-V measurements for the glass/FTO/n-CdS/n-CdTe/p-CdTe/Au devices were performed under both dark and A.M1.5 illuminated conditions. Figure 7 (a) shows a typical band diagram of the g/FTO/n-CdS/n-CdTe/p-CdTe/Au thin film solar cell, while, Figure 7 (b) and (c) show both the linear-linear and log-linear I-V curve of the pH2 $CdCl_2$ treated glass/FTO/*n*-CdS/*n*-CdTe/*p*-CdTe/Au devices respectively. Figure 7 (d) shows the I-V curves taken under A.M1.5 illumination condition for the glass/FTO/*n*-CdS/*n*-CdTe/*p*-CdTe/Au devices treated with different pH of $CdCl_2$. While *Table 3* shows the summary of the electronic properties of the glass/FTO/n-CdS/n-CdTe/*p*-CdTe/Au devices fabricated. From the I-V data obtained under dark condition, electrical properties such as the shunt resistance R_{sh}, series resistance R_s, rectification factor *RF*, reverse saturation current

I_o, ideality factor n, and the barrier height ϕ_b were derived, while the effective Richardson constant (A^*) for CdTe was calculated to be 12 $Acm^{-2}K^{-2}$. As observed in *Table 3*, the R_{sh} was comparatively high for all the pH values explored in this work but a noticeable reduction of about two orders of magnitude was observed at pH1.

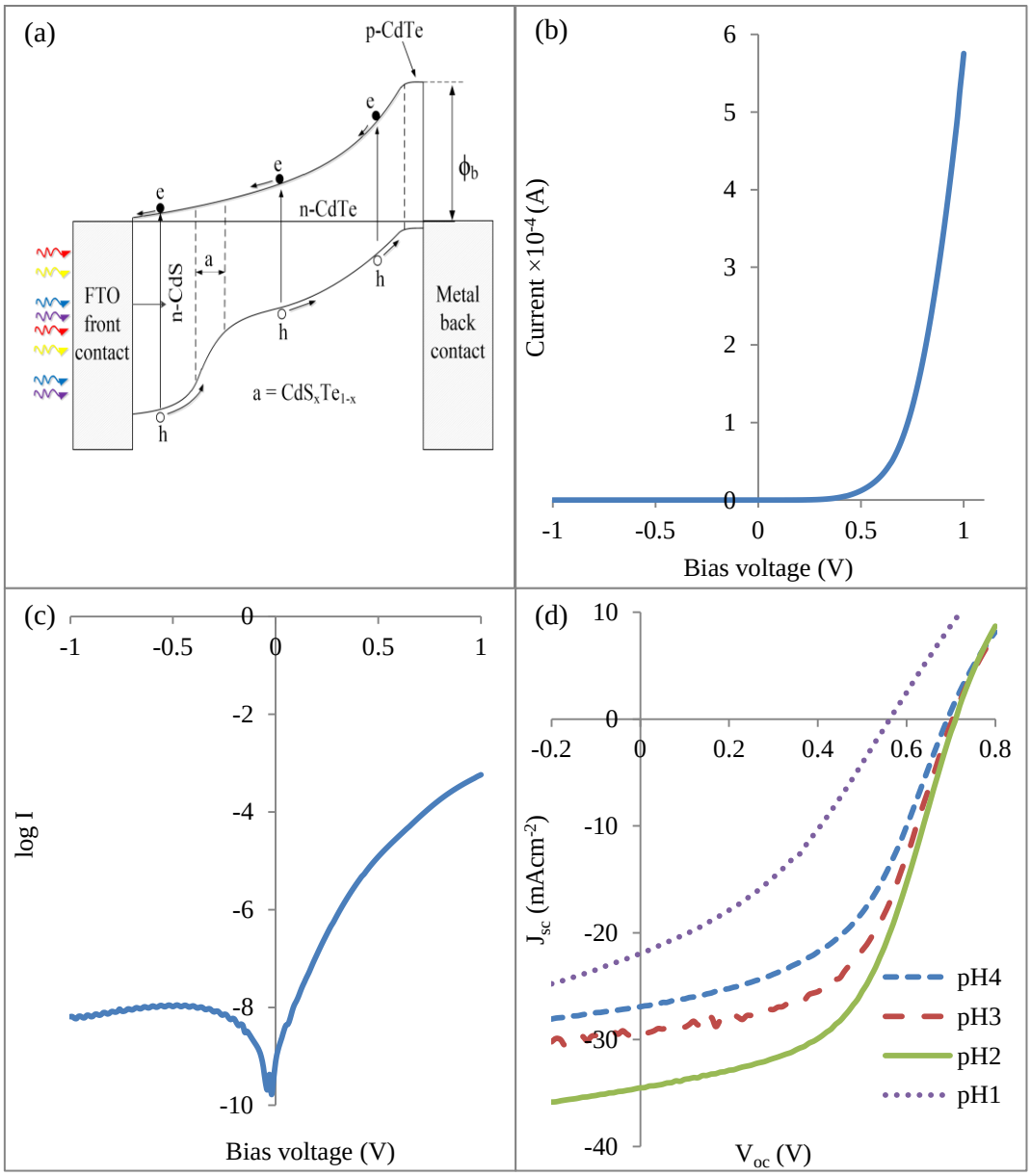

Figure 7: (a) The band diagram of the g/FTO/n-CdS/n-CdTe/p-CdTe/Au thin film solar cell (b) Typical linear–linear I–V curve and (c) semi-logarithmic current versus voltage curve measured under dark conditions for glass/FTO/n-CdS/n-CdTe/p-CdTe/Au devices. (the layers were treated with pH2 $CdCl_2$). (d) Linear I–V curve of glass/FTO/n-CdS/n-CdTe/p-CdTe/Au under AM 1.5 for device treated with $CdCl_2$ at pH1-pH4.

It is well known that low R_{sh} can be attributed to the low quality of the semiconductor material [25] which might be due to the inclusion of gaps, voids, pinholes, high dislocation density within the semiconductor material [25]. Based on this, it can be deduced that the semiconductor material quality at pH1 has been reduced. Interestingly, this observation is in accord with the analytical studies as discussed Sections 3.1 - 3.3.

Furthermore, the glass/FTO/*n*-CdS/*n*-CdTe/*p*-CdTe/Au device activated using $CdCl_2$ at pH2, pH3 and pH4 shows *log RF* values of above 3 with a tendency for archiving highly efficient solar cell [26]. On the contrary, the low *log RF* values observed for glass/FTO/*n*-CdS/*n*-CdTe/*p*-CdTe/Au device activated using $CdCl_2$ at pH1 shows lower *log RF* value of 1.27 which indicates the inability of the fabricated device to achieve high efficiencies. This observation might be due to the dominance of the current transport mechanism by recombination and generation (R&G) centres as indicated by *n* value >2. It should be noted that for an ideal diode, the ideality factor *n* is 1.00 indicating the dominance of the current transportation mechanism by thermionic emission. But if the ideality factor falls between 1.00 and 2.00, the current transportation mechanism is dominated by both thermionic emission and R&G centres. As reported by Verschraegen et al, the current transportation mechanism of a diode with an ideality factor above 2 is dominated with high-energy electrons tunnelling through the barrier high in addition to both thermionic emission and R&G mechanisms [27]. The current transport mechanism of *n*>2 might result in barrier high ϕ_b reduction as observed in Table 3 for the pH1 $CdCl_2$ activated device.

Table 3: Summary of Device parameters from I–V (dark conditions), I–V (illuminated at AM1.5) and C–V (dark conditions) measurements.

$CdCl_2$ post-growth treatment pH	1	2	3	4
I-V under Dark condition				
$R_{sh} \times 10^5$ (Ω)	0. 08	10.13	5.72	5.28
$R_s \times 10^3$ (Ω)	1.27	0.47	0.87	0.89
log RF	1.40	4.80	3.50	3.50
$I_o \times 10^{-9}$ (A)	158.49	1.00	3.98	3.16
n	>2.00	1.60	1.86	1.91
Φ_b (eV)	>0.67	>0.80	>0.77	>0.77
I-V under A.M1.5 illuminated condition				
J_{sc} ($mAcm^{-2}$)	21.66	35.03	29.62	27.39
V_{oc} (V)	0.58	0.72	0.71	0.70
FF	0.40	0.52	0.55	0.52
η (%)	5.00	13.10	11.60	10.00
C-V under dark condition				
$\sigma \times 10^{-5}$ $(\Omega.cm)^{-1}$	8.97	40.63	33.80	24.33
$N_D \times 10^{14}$ (cm^{-3})	254.00	1.95	3.66	6.67
μ ($cm^2V^{-1}S^{-1}$)	0.02	13.00	5.76	2.28

Under A.M1.5 condition as shown in Figure 7 (d) and Table 3, the observed J_{sc} of cell treated using pH1 CdTe post-growth-treatment is relatively lower than pH2, pH3 and pH4. This observation can be related to the high ideality factor as a result of high R&G centre intensity. It should be noted that the J_{sc} observed in this work is higher than the Shockley– Queisser limit of a single *p–n* junction [28] due to the multi-layer and multi-junction *n–n–p* device configuration [29]. The explored glass/FTO/*n*-CdS/*n*-CdTe/*p*-CdTe/Au cells were isolated by carefully removing surrounding layers to ensure that there was no peripheral collection as suggested by Godfrey et al [30]. Although no peripheral collection of the current was expected due to the high resistivity and ultra-thin layer (total thickness <1500 nm) utilised in this work [31]. Using the multilayer configuration, the main author's group have reported 140% IPCE measurement value owing to the incorporation of impurity PV effect and impact ionisation [32], while, other independent researchers have also report EQE values above 100% [33], [34].

Comparatively, similar V_{oc} was observed for glass/FTO/*n*-CdS/*n*-CdTe/*p*-CdTe/Au layers treated with $CdCl_2$ at pH2 to pH4 while a reduction in the V_{oc}, *FF* and η of the layers treated with pH1 CdTe were observed. These observations were been anticipated due the degradation of the material quality, reduction in crystallinity, conductivity type transition and high resistivity based on the analysis in Sections 3.1 - 3.5 respectively.

3.6.2 CAPACITANCE - VOLTAGE CHARACTERISTICS OF RECTIFYING CONTACTS

Figure 8 (a) and (b) show the capacitance–voltage (*C*-*V*) and the Mott-Schottky (C^{-2} versus *V)* plot of the glass/FTO/*n*-CdS/*n*-CdTe/p-CdTe/Au respectively for the pH2 $CdCl_2$ treated layers. While the properties such as the doping density N_D and mobility μ for glass/FTO/*n*-CdS/*n*-CdTe/*p*-CdTe/Au devices treated with pH1 to pH4 are tabulated in Table 3. For this sets of experiments, the measurements were carried out at a frequency of 1.0 MHz between the bias voltage range of -1.00 V to 1.00 V at 300 K. The reported doping density N_D in this work was obtained using the Mott-Schottky plot as shown in Figure 8 (b) and Eq. (3)-(5). Where *C* is the capacitance, V_{bi} is the built-in potential, V_R is the reverse bias voltage, *A* is the area of the contact, *e* is the electronic charge, ε_o is the permittivity of free space, ε_s is the semiconductor permittivity and ε_r is the relative permittivity (or dielectric constant). The ε_r value was taken to be 11 [35], while, the slope obtained from the intercept of the Mott-Schottky plot as shown in Figure 8 (b) was incorporated into Eq. (4).

$$C^{-2} = \frac{2}{\varepsilon_s e A^2 N_D}(V_R + V_{bi}) \tag{3}$$

$$N_D = \frac{2}{\varepsilon_r \varepsilon_o e A^2 * slope} \tag{4}$$

$$slope = \frac{2}{\varepsilon_s e N_D A^2} \tag{5}$$

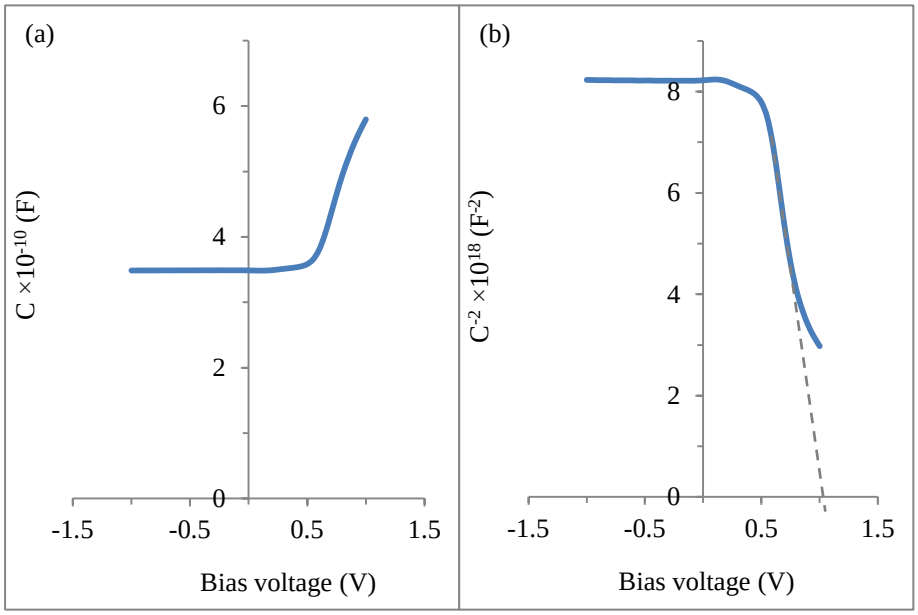

Figure 8: A typical (a) Capacitance-voltage and (b) Schottky–Mott plot of the glass/FTO/n-CdS/n-CdTe/p-CdTe/Au layer treated with pH2 $CdCl_2$.

Using Eq. (6) the effective density of states N_c was calculated to be 9.15×10^{17} cm^3, where h is the Plank's constant, m_e^* is the effective electron mass, T is the temperature at 300K and k is the Boltzmann's constant. The electron mobility μ was calculated using Eq. (7).

$$N_c = 2\left[\frac{2\pi m_e^* kT}{h^2}\right]^{\frac{3}{2}} \tag{6}$$

$$\mu_\perp = \frac{\sigma}{N_D e} \tag{7}$$

As observed in Figure 8, the fabricated device treated with $CdCl_2$ at pH2 was fully depleted at the reverse through the zero and towards ~0.5V in the forward bias with the depletion width W equalling to the fabricated device thickness of ~1350 nm. Increasing the voltage in the forward bias to ~0.5V and above, a gradual reduction in the depletion width was observed with a corresponding increase in capacitance. This observation was similar for glass/FTO/*n*-CdS/*n*-CdTe/p-CdTe/Au devices treated with $CdCl_2$ at pH3 and pH4. Furthermore, the calculated N_D in Table 3 for the devices treated with $CdCl_2$ at pH2 - pH4 are of the same order of magnitude

(10^{14} cm^{-3}). High-efficiency solar cells have been reported to have N_D values within the (~1.0×10^{14} – 5×10^{15} cm^{-3}) [36], [37]. The N_D value of the devices activated with $CdCl_2$ at pH1 signifies high doping which might result to a loss of J_{sc}, incorporation of defects within the crystal lattice, shrinkage of the depletion width and the consequent reduction in the photo-generated current collection efficiency [38]. These observations coupled with the high defect density (R&G) centres might be the cause of the reduction in the charge carrier mobility of the devices activated with pH1 $CdCl_2$ as compared to pH2 – pH4 $CdCl_2$ treatment acidity.

4 CONCLUSION

In conclusion, this experimental work has explored the effect of $CdCl_2$ post-growth-treatment pH on both material and fabricated CdS/CdTe device properties. It was observed that better material and device properties can be achieved at pH2 $CdCl_2$ activation treatment. Although, the device parameter such as the V_{oc} shows no distinct difference after treatment with pH2-pH4 $CdCl_2$, the $CdCl_2$ treatment at pH1 shows comparable low-quality material quality as observed in the structural, morphological and compositional properties while the overall fabricated device photon-to-electron efficiency was low. Work is on-going on optimising other processing step towards achieving higher efficiencies.

CONFLICT OF INTEREST

We have no conflict of interest in this paper.

ACKNOWLEDGEMENT

Authors will like to thank members of the SHU Solar Energy Group comprising of Salim Hussein, Olusola Olajide, Azlian Abdul-Manaf and Mohammed Madugu for their contributions to this work. The principal author will also like to thank Sheffield Hallam University, Ekiti State University and TETFund Nigeria for their support.

REFERENCES

[1] I. M. Dharmadasa, "Review of the CdCl2 Treatment Used in CdS/CdTe Thin Film Solar Cell Development and New Evidence towards Improved Understanding," *Coatings*, vol. 4, no. 2, pp. 282–307, 2014.

[2] S. Mazzamuto, L. Vaillant, A. Bosio, N. Romeo, N. Armani, and G. Salviati, "A study of the CdTe treatment with a Freon gas such as CHF2Cl," *Thin Solid Films*, vol. 516, pp. 7079–7083, 2008.

[3] J. D. Major, L. Bowen, R. E. Treharne, L. J. Phillips, and K. Durose, "NH 4 Cl Alternative to the CdCl 2 Treatment Step for CdTe Thin-Film Solar Cells," *IEEE J.*, vol. 5, no. 1, pp. 386–389, 2015.

[4] B. Maniscalco, A. Abbas, J. W. Bowers, P. M. Kaminski, K. Bass, G. West, and J. M. Walls, "The activation of thin film CdTe solar cells using alternative chlorine containing compounds," *Thin Solid Films*, vol. 582, pp. 115–119, 2015.

[5] A. Bosio, N. Romeo, S. Mazzamuto, and V. Canevari, "Polycrystalline CdTe thin films for photovoltaic applications," *Prog. Cryst. Growth Charact. Mater.*, vol. 52, no. 4, pp. 247–279, 2006.

[6] B. M. Başol, "Processing high efficiency CdTe solar cells," *Int. J. Sol. Energy*, vol. 12, no. 1–4, pp. 25–35, 1992.

[7] B. E. McCandless, I. Youm, and R. W. Birkmire, "Optimization of vapor post-deposition processing for evaporated CdS/CdTe solar cells," *Prog. Photovoltaics Res. Appl.*, vol. 7, no. 1, pp. 21–30, 1999.

[8] H. Bayhan and C. Erc?elebi, "Effects of Post Deposition Treatments on Vacuum Evaporated CdTe Thin Films and CdS/CdTe Heterojunction Devices," *Turkish J. Phys.*, vol. 22, pp. 441–451, 1998.

[9] N. A. Abdul-Manaf, A. R. Weerasinghe, O. K. Echendu, and I. M. Dharmadasa, "Electro-plating and characterisation of cadmium sulphide thin films using ammonium thiosulphate as the sulphur source," *J. Mater. Sci. Mater. Electron.*, vol. 26, no. 4, pp. 2418–2429, 2015.

[10] H. Lin, Irfan, W. Xia, H. N. Wu, Y. Gao, and C. W. Tang, "MoOx back contact for CdS/CdTe thin film solar cells: Preparation, device characteristics, and stability," *Sol. Energy Mater. Sol. Cells*, vol. 99, pp. 349–355, 2012.

[11] A. A. Ojo and I. M. Dharmadasa, "15.3% efficient graded bandgap solar cells fabricated using electroplated CdS and CdTe thin films," *Sol. Energy*, vol. 136, pp. 10–14, 2016.

[12] H. I. Salim, V. Patel, a. Abbas, J. M. Walls, and I. M. Dharmadasa, "Electrodeposition of CdTe thin films using nitrate precursor for applications in solar cells," *J. Mater. Sci. Mater. Electron.*, vol. 26, no. 5, pp. 3119–3128, 2015.

[13] J. Woodcock, A. Turner, M. Ozsan, and J. Summers, “Thin film solar cells based on electrodeposited CdTe,” in *The Conference Record of the Twenty-Second IEEE Photovoltaic Specialists Conference - 1991*, 1991, pp. 842–847.

[14] I. M. Dharmadasa, C. J. Blomfield, C. G. Scott, R. Coratger, F. Ajustron, and J. Beauvillain, “Metal/n-CdTe interfaces: A study of electrical contacts by deep level transient spectroscopy and ballistic electron emission microscopy,” *Solid. State. Electron.*, vol. 42, no. 4, pp. 595–604, Apr. 1998.

[15] I. M. Dharmadasa, “Recent developments and progress on electrical contacts to CdTe, CdS and ZnSe with special reference to barrier contacts to CdTe,” *Prog. Cryst. Growth Charact. Mater.*, vol. 36, no. 4, pp. 249–290, Jan. 1998.

[16] J. Tauc and A. Menth, “States in the gap,” *J. Non. Cryst. Solids*, vol. 8–10, pp. 569–585, 1972.

[17] V. Krishnakumar, J. Han, A. Klein, and W. Jaegermann, “CdTe thin film solar cells with reduced CdS film thickness,” *Thin Solid Films*, vol. 519, no. 21, pp. 7138–7141, 2011.

[18] D. A. Wood, K. D. Rogers, D. W. Lane, D. A. Wood, K. D. Rogers, and J. A. Coath, “Optical and structural characterization of CdS x Te 1- x thin films for solar cell applications,” *J. Phys. Condens. Matter*, vol. 12, no. 19, p. 4433, 2000.

[19] G. Carotenuto, M. Palomba, S. De Nicola, G. Ambrosone, and U. Coscia, “Structural and Photoconductivity Properties of Tellurium/PMMA Films.,” *Nanoscale Res. Lett.*, vol. 10, no. 1, p. 1007, 2015.

[20] B. Abad, M. Rull-Bravo, S. L. Hodson, X. Xu, and M. Martin-Gonzalez, “Thermoelectric properties of electrodeposited tellurium films and the sodium lignosulfonate effect,” *Electrochim. Acta*, vol. 169, pp. 37–45, Jul. 2015.

[21] S. Chun, S. Lee, Y. Jung, J. S. Bae, J. Kim, and D. Kim, “Wet chemical etched CdTe thin film solar cells,” *Curr. Appl. Phys.*, vol. 13, no. 1, pp. 211–216, 2013.

[22] J. Nowotny, T. Bak, M. Nowotny, and L. Sheppard, “Titanium dioxide for solar-hydrogen I. Functional properties☆,” *Int. J. Hydrogen Energy*, vol. 32, no. 14, pp. 2609–2629, 2007.

[23] N. Abdul-Manaf, H. Salim, M. Madugu, O. Olusola, and I. Dharmadasa, “Electro-Plating and Characterisation of CdTe Thin Films Using CdCl2 as the Cadmium Source,” *Energies*, vol. 8, no. 10, pp. 10883–10903, 2015.

[24] P. J. Sellin, A. W. Dazvies, A. Lohstroh, M. E. Özsan, and J. Parkin, “Drift mobility and mobility-lifetime products in CdTe:Cl grown by the travelling heater method,” *IEEE Trans. Nucl. Sci.*, vol. 52,

no. 6, pp. 3074–3078, 2005.

[25] T. Soga, “Nanostructured Materials for Solar Energy Conversion,” *Elsvier Sci.*, vol. 2030, p. 614, 2004.

[26] I. M. Dharmadasa, *Advances in thin-film solar cells*. Singapore: Pan Stanford, 2013.

[27] J. Verschraegen, M. Burgelman, and J. Penndorf, “Temperature dependence of the diode ideality factor in CuInS2-on-Cu-tape solar cells,” *Thin Solid Films*, vol. 480–481, pp. 307–311, 2005.

[28] W. Shockley and H. J. Queisser, “Detailed Balance Limit of Efficiency of p-n Junction Solar Cells,” *J. Appl. Phys.*, vol. 32, no. 3, p. 510, 1961.

[29] A. De Vos, “Detailed balance limit of the efficiency of tandem solar cells,” *J. Phys. D. Appl. Phys.*, vol. 13, no. 5, pp. 839–846, 2000.

[30] R. B. Godfrey and M. A. Green, “Enhancement of MIS solar-cell ‘efficiency’ by peripheral collection,” *Appl. Phys. Lett.*, vol. 31, no. 10, pp. 705–707, 1977.

[31] B. M. Basol, “High-efficiency electroplated heterojunction solar cell,” *J. Appl. Phys.*, vol. 55, no. 1984, pp. 601–603, 1984.

[32] I. M. Dharmadasa, A. A. Ojo, H. I. Salim, and R. Dharmadasa, “Next generation solar cells based on graded bandgap device structures utilising rod-type nano-materials,” *Energies*, vol. 8, no. 6, pp. 5440–5458, 2015.

[33] D. Congreve, J. Lee, N. Thompson, and E. Hontz, “External Quantum Efficiency Above 100% in a Singlet-Exciton-Fission–Based Organic Photovoltaic Cell,” *Science (80-.).*, vol. 340, no. 6130, pp. 334–337, 2013.

[34] N. J. L. K. Davis, M. L. Bohm, M. Tabachnyk, F. Wisnivesky-Rocca-Rivarola, T. C. Jellicoe, C. Ducati, B. Ehrler, and N. C. Greenham, “Multiple-exciton generation in lead selenide nanorod solar cells with external quantum efficiencies exceeding 120%,” *Nat Commun*, vol. 6, no. 2, pp. 81–87, Sep. 2015.

[35] I. Strzalkowski, S. Joshi, and C. R. Crowell, “Dielectric constant and its temperature dependence for GaAs, CdTe, and ZnSe,” *Appl. Phys. Lett.*, vol. 28, no. 6, pp. 350–352, Mar. 1976.

[36] B. M. Basol and B. McCandless, “Brief review of cadmium telluride-based photovoltaic technologies,” *J. Photonics Energy*, vol. 4, p. 40996, 2014.

[37] M. Gloeckler, I. Sankin, and Z. Zhao, “CdTe solar cells at the threshold to 20% efficiency,” *IEEE J. Photovoltaics*, vol. 3, no. 4, pp. 1389–1393, 2013.

[38] T. J. Coutts and S. Naseem, “High Efficiency Indium Tin Oxide/Indium Phosphide Solar Cells.,” *Appl. Phys. Lett.*, vol. 46, no. 2, pp. 164–166, 1985.

LIST OF FIGURES